EURASIAN PHYSICAL TECHNICAL JOURNAL

2026, Volume 23, No. 2 (56)

https://doi.org/10.31489/2026N2/139-147

Received: 13/02/2026 Revised: 28/05/2026 Accepted: 26/06/2026 Published online: 30/06/2026

Original Research Article

UDC 53.03; 52-17; 524.7-1/-8

PROBING KING AND PLUMMER DARK MATTER MODELS USING ROTATION CURVES

Kurmanov Ye.[1,2], Konysbayev T.[1,2], Suliyeva G.[1,2,3]*, Urazalina A.[1,2], Oteev T.[4], Rabigulova G.[2], Nurlanbek U.[2], Adil M.[2], Bekmurat B.[2], Tuzen G.[2]

[1] National Nanotechnology Laboratory of Open Type, Almaty, Kazakhstan
[2] Al-Farabi Kazakh National University, Almaty, Kazakhstan
[3] Fesenkov Astrophysical Institute, Almaty, Kazakhstan
[4] Nukus State Pedagogical Institute, Nukus, Uzbekistan
*Corresponding author: g_suliyeva@mail.ru

Abstract. *In this work, we study the distribution of dark matter in the halos of the spiral galaxies ESO3050090, ESO4880049, and ESO0140040 using their observed rotation curves. The analysis adopts spherically symmetric dark matter halos described by the King and Plummer density profiles, neglecting the baryonic component to emphasize the influence of the halo component only. As a first step, the characteristic halo parameters, the central density and the scale radius, are determined through a nonlinear least-squares fitting procedure based on the Levenberg–Marquardt algorithm. These best-fit values are then used as initial conditions for the Markov Chain Monte Carlo method to estimate the parameter space and uncertainties. Subsequently, we compare the results obtained from two specified fitting methods to assess their consistency and robustness. A statistical comparison between the King and Plummer profiles is performed using the Bayesian Information Criterion. The results of this work clarify how effectively the halo models under consideration reproduce the observed kinematics and highlight the ability to distinguish alternative dark matter density profiles.*

Keywords: dark matter, spiral galaxies, rotation curves, King profile, Plummer profile.

1. Introduction

Dark matter (DM) accounts for approximately 27% of the total energy density of the Universe and plays a key role in the formation and dynamical evolution of galaxies and galaxy clusters [1–4]. Its existence is supported by several independent observational probes, including galaxy rotation curves (RCs), strong and weak gravitational lensing, and measurements of the cosmic microwave background. Together, these observations consistently indicate mass distributions that significantly exceed the baryonic component alone [5, 6]. The galactic RCs serving as one of the most direct observational signatures of DM [7] show how the orbital velocity of stars and gas varies with distance from the galactic center. Their analysis allows not only to confirm the presence of DM but also to quantitatively constrain its radial distribution within individual galaxies [8, 9]. This is a fundamental problem in astrophysics, since the DM component governs the gravitational potential and thereby controls the observed galactic dynamics.

A variety of halo density profiles has been introduced in the literature to describe the mass distributions inferred from RC data. Among the most widely used models is the Navarro–Frenk–White (NFW) profile, derived by Navarro et al. [10] from N-body simulations within the standard cold DM framework. In contrast, Burkert [11] introduced a phenomenological cored profile to reproduce the observed RCs of dwarf spiral galaxies. Jimenez et al. [12] demonstrated that a large sample of galaxy RCs can be satisfactorily fitted using

the pseudo-isothermal profile. Brownstein [13] further showed that a core-modified profile with a constant central density provides a good description of the RCs of both high- and low-surface brightness galaxies.

In Refs. [14, 15], the RC data of the low-surface-brightness (LSB) galaxies U11819, U5750, U11454, and U11648 were investigated by some of us, assuming a spherically symmetric distribution of DM. The free parameters of several well-known phenomenological DM density profiles were obtained by fitting the observed RCs using least-squares techniques and the Markov Chain Monte Carlo (MCMC) method. The Bayesian Information Criterion (BIC) was employed to identify the best-fitting models for each galaxy, showing that different density profiles provide the optimal description for different systems.

In addition, in Ref. [16], the RC of the galaxy ESO0140040 was analyzed to investigate the imprint of non-vanishing DM pressure on halo properties. Several phenomenological density profiles were tested using least-squares fitting and information criteria, showing that cored profiles, such as the pseudo-isothermal and Einasto models, provide the most suitable framework for studying the DM equation of state, while cuspy profiles are disfavored.

In Ref. [17], the RCs of the Andromeda galaxy and the Milky Way were analyzed from the central regions to the outer halo within a multi-component mass model. The bulge and disk were described using exponential sphere profiles, while several phenomenological DM halo models were tested in the outer regions. A statistical comparison based on the BIC demonstrated that the exponential sphere profile provides the most consistent description of both galaxies, outperforming cuspy and de Vaucouleurs-type models. The analysis also showed that the choice of the halo profile affects the inferred inner structure and global mass distribution, with the Milky Way found to be less massive than Andromeda, in agreement with independent studies.

Finally, extending these studies to the physical properties of DM, in previous work [18], the DM distribution in the galactic core and inner regions was described by an exponential sphere profile and compared with the Einasto, Burkert, and isothermal halo models. In another work [19], through the statistical analysis for several LSB galaxies, phenomenological profiles were compared to the profiles derived within the framework of Scalar Field Dark Matter (SFDM) model.

In this work, we study the DM distribution in the halos of LSB galaxies ESO3050090, ESO4880049, and ESO014004 based on their observed RCs. LSB galaxies are valuable for halo studies, since their dynamical mass is commonly inferred to be dominated by DM [20, 21]. Moreover, the three galaxies considered here exhibit different RC morphologies and characteristic velocity scales, which allows us to test the ability of the adopted halo models to reproduce distinct kinematic regimes within a single fitting framework.

To model the halo density distribution, we employ King and Plummer density profiles. These two models represent cored density distributions which makes them useful for testing systems where observations indicate finite densities in the inner regions, in contrast to cuspy profiles predicted by cold dark matter (CDM) simulations. Unlike other cored DM profiles (for example, Burkert, pseudo-isothermal, Exponential Sphere, Brownstein profiles), which have been extensively studied in the literature, the King and Plummer profiles have received considerably less attention in this context. And their ability to reproduce observed RCs of LSB galaxies remained poorly constrained.

The observational RC data used in our analysis are taken from Refs. [22, 23]. To compare the results, we apply two complementary fitting techniques: a nonlinear least-squares method based on the Levenberg–Marquardt algorithm and the MCMC approach. The nonlinear fit is first used to obtain preliminary parameter estimates and to identify the minimum χ^2 solution. These values are then adopted as initial conditions and prior ranges for the MCMC analysis, which provides the best-fitting models and reliable uncertainties. On the basis of the resulting density profiles, we subsequently compute the DM mass enclosed within the halos of the galaxies.

This paper is organized as follows. In Section 2, we introduce the DM density profiles adopted in the analysis. Section 3 is devoted to the description of fitting procedures. Section 4 presents the corresponding numerical results and discussion. The main conclusions of the study are summarized in Section 5.

2. Dark Matter halo density profiles

In this section, we present the DM density profiles used in this work. Modeling the mass distribution of galactic DM halos is commonly performed by specifying an analytical form for the density $\rho(r)$, which serves as the starting point for constructing the corresponding gravitational potential and predicted RC. Different profiles correspond to different assumptions about the behavior of the DM density in the central and outer regions of galaxies.

RC data indicate that the DM density is not uniform and varies with radius. To examine how the choice of the profile affects the results, we consider the DM density models introduced below.

King profile [24]:

$$\rho_K(r) = \rho_0 \left(1 + \frac{r^2}{r_0^2}\right)^{-3/2}. \quad (1)$$

Plummer profile [25]:

$$\rho_P(r) = \rho_0 \left(1 + \frac{r^2}{r_0^2}\right)^{-5/2}, \quad (2)$$

where ρ_0 is the central density of DM, and r_0 is the scale radius. These profiles are characterized by smooth behavior at the origin and contain two free parameters ρ_0 and r_0.

The distinction between the King and Plummer models lies in their outer density slopes. At large radii, the King profile decreases as a power law with $\rho_K(r) \sim r^{-3}$. This relatively shallow decline implies an extended halo structure and allows the profile to reproduce slowly varying or approximately flat RCs over a broad radial interval. The Plummer model exhibits a sharper decline at large radii, with $\rho_P(r) \sim r^{-5}$, which leads to a more centrally concentrated halo.

3. Methods

Using the RC data of ESO3050090, ESO4880049 and ESO014004, we examined the properties of their halos by employing two complementary fitting methods.

In the first stage, we applied the nonlinear least-squares procedure (Levenberg–Marquardt) to obtain initial estimates for the free parameters of the selected density profiles. This step helps to identify the region where the χ^2 function is minimized and provides suitable starting values for the subsequent analysis.

We then performed a MCMC study. Unlike the initial fit, the MCMC method explores the parameter space more extensively and allows us to determine statistically reliable intervals for the parameters in both density profiles. The MCMC output refines the preliminary values obtained from the nonlinear approach and shows how accurately each profile follows the observed RCs.

Since the central parts of ESO3050090, ESO4880049, and ESO0140040 remain poorly constrained, we limit the analysis to the halo component and use

$$v_{tot}^2(r) \simeq v_{profile}^2(r), \quad (3)$$

where $v_{profile}(r)$ is the circular velocity of the DM halo.

The circular velocity associated with a given halo mass profile $M(r)$ is

$$v_{profile}(r) = \sqrt{\frac{GM(r)}{r}}. \quad (4)$$

Mass profile is

$$M(r) = 4\pi \int_0^r r^2 \rho(r) dr. \quad (5)$$

Using the density profiles given in Eqs. (1) and 2 and substituting them into Eq. (5), we obtain the corresponding mass profiles for the King and Plummer models.

$$M_{King}(r) = 4\pi r_0^3 \rho_0 \left(-\frac{r}{\sqrt{r^2 + r_0^2}} + \operatorname{arcsinh}\left(\frac{r}{r_0}\right) \right). \quad (6)$$

$$M_{Plummer}(r) = \frac{4\pi \rho_0 r^3 r_0^3}{3\left(r^2 + r_0^2\right)^{3/2}}. \quad (7)$$

To identify which of the two models provides a better description of the RCs of ESO3050090, ESO4880049 and ESO0140040, we compared their fits using the BIC. For each density profile, the value of BIC was calculated as

The Bayesian Information Criterion (BIC) was used to compare the considered dark matter models. For the MCMC analysis, the BIC was estimated as

$$BIC = \chi^2 + k \ln N, \quad (8)$$

where χ is the minimum chi-square value, k is the number of free parameters, and N is the number of observational data points.

For the nonlinear fitting analysis, the BIC values were obtained directly from the built-in Mathematica routine *NonlinearModelFit*, which evaluates the likelihood-based criterion

$$BIC = -2 \ln L_{\max} + k \ln N, \quad (9)$$

where $L_{\max}$ is the maximum likelihood. Assuming Gaussian observational errors,

$$-2\ln L_{\max} = \chi^2 + \sum_{i=1}^{N} \ln(2\pi\sigma_i^2), \quad (10)$$

where σ_i denotes the uncertainty associated with the i-th observational data point. Therefore, the likelihood-based BIC values used in the nonlinear fitting analysis are not necessarily identical to those estimated directly from χ.

The parameter estimation was performed using the Metropolis–Hastings algorithm. Uniform priors were adopted for all free parameters within fixed physically motivated ranges. The prior intervals were chosen to define the allowed parameter space for each model. Initial parameter estimates obtained from the nonlinear least-squares fit were used only as starting values and for selecting reasonable parameter ranges.

For the King profile, the prior ranges were chosen as $\rho_0 \in [1, 250]$ and $r_0 \in [1, 10]$, while for the Plummer profile they were $\rho_0 \in [1, 349]$ and $r_0 \in [1, 13]$. A preliminary MCMC run was used to estimate the proposal covariance matrix, followed by a production chain of 50,000 steps. The initial part of the chain was discarded as burn-in before calculating the final parameter estimates and confidence intervals. Convergence was assessed by inspecting the trace plots of the sampled parameters and the corresponding χ. values.

For practical comparison, we introduce the relative quantity

$$\Delta BIC = BIC - BIC_{min}, \quad (11)$$

where BIC_{min} is the smallest value among all competing models.

For completeness, the likelihood-based BIC values obtained from the built-in Mathematica routine NonlinearModelFit are 74.17and 79.09for ESO0140040, 79.02and 81.30for ESO3050090, and 59.41and 67.80for ESO4880049. The reported ΔBICvalues were computed directly from these likelihood-based BIC values.

For the MCMC analysis, the corresponding BIC values are 9.12 and 13.34 for ESO0140040, 6.59 and 8.87 for ESO3050090, and 7.92 and 16.31 for ESO4880049, obtained using Eq. (8).

Prior to performing the MCMC analysis, we first identified the region where the χ^2 function reaches its minimum by applying the nonlinear Levenberg–Marquardt method. This preliminary step yields a reasonable starting point for the model parameters. In this procedure, the quantity being minimized is

$$\chi^2 = \sum_{i=1}^{N} \left[\frac{v_i^{obs} - v(\rho_0, r_0, r)}{\sigma_{v,i}^{obs}}\right]^2, \quad (12)$$

where v_i^{obs} are the measured rotation velocities and $v(\rho_0, r_0, r)$ is the model velocity computed from the assumed halo profile.

4. Results and discussion

In the left panels of Figures 1, 2, 3, the RCs of the galaxies ESO3050090, ESO4880049 and ESO0140040 are shown together with the model curves obtained from the two halo profiles examined in this work. In all three cases, the blue points represent the observed rotation velocities, and the vertical bars mark the corresponding measurement errors.

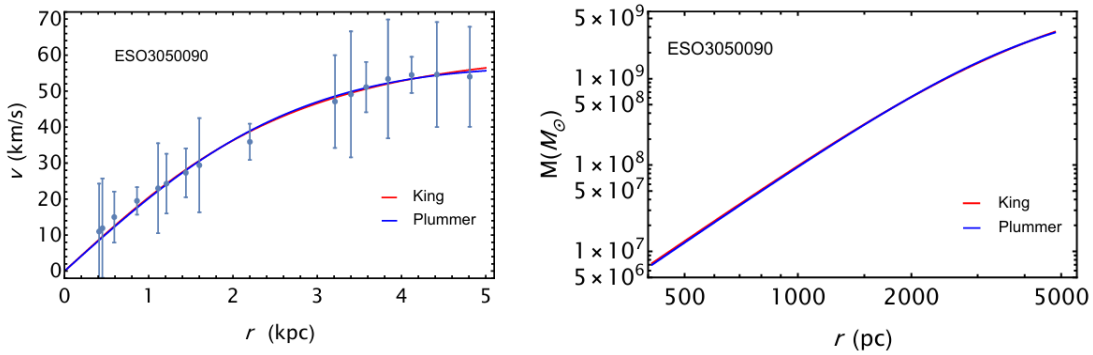

Fig.1. Left panel: Best fit velocity profile for ESO3050090 galaxy. Right panel: Logarithmic mass profiles of DM in the halo in ESO3050090 galaxy.

The solid lines indicate the best-fit King (red) and Plummer (blue) solutions. As the figures show, both halo models follow the general rise of the RCs for each galaxy and reproduce the data within the reported errors over the radial range covered by the observations. This agreement confirms that considered galaxies are

dominated by DM over the observed radial range, and the baryonic contributions are subdominant. In addition, the graphical results show that cored profiles are quite preferable for describing LSB galaxies. Figure 4 shows the contour plots for the parameters ρ_0 and r_0 obtained from the MCMC analysis for the galaxies ESO3050090, ESO0140040 and ESO4880049.

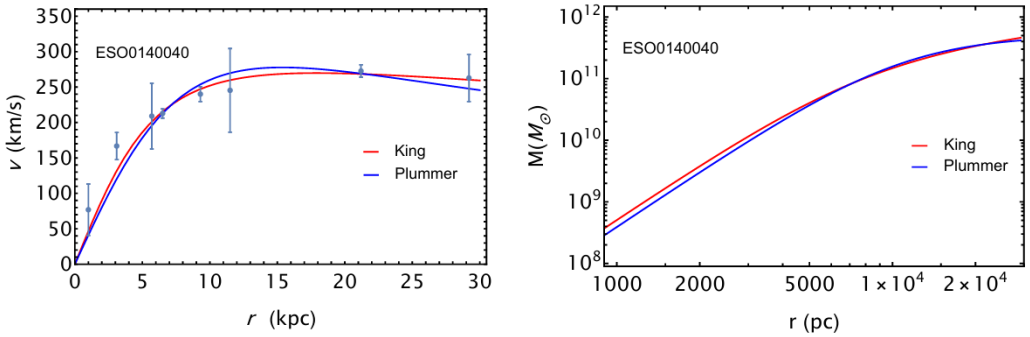

Fig.2. Left panel: Best fit velocity profile for ESO0140040 galaxy. Right panel: Logarithmic mass profiles of DM in the halo in ESO0140040 galaxy.

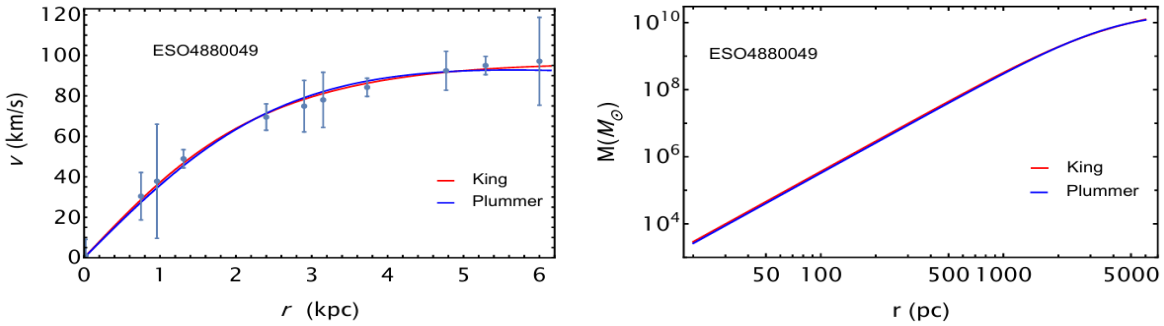

Fig.3. Left panel: Best fit velocity profile for ESO4880049 galaxy. Right panel: Logarithmic mass profiles of DM in the halo in ESO4880049 galaxy.

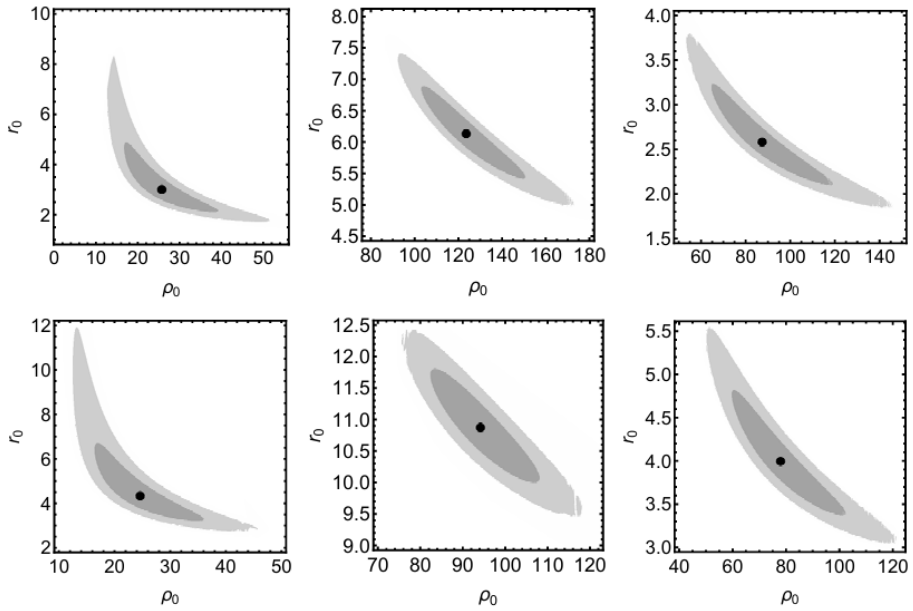

Fig.4. Contour plots of the best-fit parameters (black dots) and the associated 1σ (dark gray) and 2σ (light gray) confidence regions obtained from the MCMC analysis. From left to right, the panels correspond to the galaxies ESO3050090, ESO0140040, and ESO4880049. Top row: King profile; bottom row: Plummer profile.

Each panel corresponds to one of the two halo models considered in this work. The black point marks the best-fit parameter values. The shaded regions indicate the 1σ (dark) and 2σ (light) levels extracted from the

MCMC chains. The shape of the contours reveals an anticorrelation between ρ_0 and r_0, so larger scale radii correspond to lower central densities, and the combination $\rho_0 r^3$ determining the mass scale remains nearly constant. The mass profiles for all three galaxies: ESO3050090, ESO4880049 and ESO0140040 are shown in the right panels of Figures 1, and 2, 3. The functions $M(r)$ were obtained by substituting the King and Plummer density profiles into the integral expression given in Eq. (5). The profiles are plotted on a logarithmic scale, which makes it clear that the enclosed mass increases with radius in both models.

The results obtained from the MCMC analysis for the galaxies considered in this work are summarized in Tables 1, 3 and 5, while the corresponding parameters derived using the nonlinear fitting procedure are reported in Tables 2, 4, and 6. In all tables, we list the central density ρ_0, the characteristic scale radius r_0, the virial mass M_{vir}, and the virial radius r_{vir}, defined as the radius within which the mean density equals 200 times the critical density of the Universe.

Table 1. The parameters of the best-fit model for galaxy ESO0140040 with MCMC.

Profiles	$\rho_0 \pm \sigma_{\rho_0}$ $(10^{-3} M_\odot/\mathrm{pc}^3)$	$r_0 \pm \sigma_{r_0}$ (kpc)	r_{vir} (kpc)	M_{vir} $(10^{11} M_\odot)$	$M \pm \sigma_M^a$ $(10^{11} M_\odot)$	$M \pm \sigma_M^b$ $(10^{11} M_\odot)$	ΔBIC	χ^2
King	$123.58^{+27.18}_{-20.55}$	$6.13^{+0.75}_{-0.71}$	100.96	8.93	4.60 ± 1.6	0.62 ± 0.35	0	4.96
Plummer	$94.17^{+13.94}_{-11.78}$	$10.87^{+0.92}_{-0.87}$	54.26	4.77	4.17 ± 1.12	1.79 ± 0.70	4.22	9.18

Table 2. Best fit model parameters for galaxy ESO0140040.

Profiles	$\rho_0 \pm \sigma_{\rho_0}$ $(10^{-3} M_\odot/\mathrm{pc}^3)$	$r_0 \pm \sigma_{r_0}$ (kpc)	r_{vir} (kpc)	M_{vir} $(10^{11} M_\odot)$	$M \pm \sigma_M^a$ $(10^{11} M_\odot)$	$M \pm \sigma_M^b$ $(10^{11} M_\odot)$	ΔBIC	χ^2
King	123.60 ± 13.62	6.13 ± 0.43	100.96	8.93	4.60 ± 0.89	0.62 ± 0.20	0	4.96
Plummer	94.17 ± 10.18	10.87 ± 0.71	54.26	4.77	4.20 ± 0.85	1.79 ± 0.53	4.92	9.18

Table 3. The parameters of the best-fit model for galaxy ESO3050090 with MCMC.

Profiles	$\rho_0 \pm \sigma_{\rho_0}$ $(10^{-3} M_\odot/\mathrm{pc}^3)$	$r_0 \pm \sigma_{r_0}$ (kpc)	r_{vir} (kpc)	M_{vir} $(10^{9} M_\odot)$	$M \pm \sigma_M^a$ $(10^{9} M_\odot)$	$M \pm \sigma_M^b$ $(10^{9} M_\odot)$	ΔBIC	χ^2
King	$25.73^{+13.44}_{-9.01}$	$2.99^{+1.88}_{-0.90}$	29.11	17.13	3.50 ± 1.86	1.51 ± 0.89	0	0.82
Plummer	$24.59^{+11.42}_{-8.20}$	$4.32^{+2.38}_{-1.12}$	16.26	7.51	3.42 ± 1.62	2.94 ± 1.53	0.13	0.95

Table 4. Best fit model parameters for galaxy ESO3050090.

Profiles	$\rho_0 \pm \sigma_{\rho_0}$ $(10^{-3} M_\odot/\mathrm{pc}^3)$	$r_0 \pm \sigma_{r_0}$ (kpc)	r_{vir} (kpc)	M_{vir} $(10^{9} M_\odot)$	$M \pm \sigma_M^a$ $(10^{9} M_\odot)$	$M \pm \sigma_M^b$ $(10^{9} M_\odot)$	ΔBIC	χ^2
King	25.67 ± 1.69	2.99 ± 0.18	29.11	17.11	3.49 ± 0.39	1.51 ± 0.41	0	0.82
Plummer	24.56 ± 1.62	4.33 ± 0.25	16.27	7.51	3.42 ± 0.40	2.94 ± 0.75	2.28	0.95

Table 5. The parameters of the best-fit model for galaxy ESO4880049 with MCMC.

Profiles	$\rho_0 \pm \sigma_{\rho_0}$ $(10^{-3} M_\odot/\mathrm{pc}^3)$	$r_0 \pm \sigma_{r_0}$ (kpc)	r_{vir} (kpc)	M_{vir} $(10^{10} M_\odot)$	$M \pm \sigma_M^a$ $(10^{10} M_\odot)$	$M \pm \sigma_M^b$ $(10^{9} M_\odot)$	ΔBIC	χ^2
King	$87.37^{+31.76}_{-22.81}$	$2.58^{+0.65}_{-0.45}$	37.82	4.49	1.25 ± 0.74	3.28 ± 3.74	0	0.81
Plummer	$77.94^{+24.34}_{-12.28}$	$3.99^{+0.83}_{-0.63}$	19.16	1.95	1.20 ± 0.64	7.34 ± 6.84	0.92	1.73

Table 6. Best fit model parameters for galaxy ESO4880049.

Profiles	$\rho_0 \pm \sigma_{\rho_0}$ $(10^{-3} M_\odot/\mathrm{pc}^3)$	$r_0 \pm \sigma_{r_0}$ (kpc)	r_{vir} (kpc)	M_{vir} $(10^{10} M_\odot)$	$M \pm \sigma_M^a$ $(10^{10} M_\odot)$	$M \pm \sigma_M^b$ $(10^{9} M_\odot)$	ΔBIC	χ^2
King	87.43 ± 5.14	2.58 ± 0.11	37.83	4.49	1.25 ± 0.12	3.28 ± 0.61	0	0.81
Plummer	78.10 ± 5.85	3.99 ± 0.19	19.14	1.94	1.20 ± 0.15	7.33 ± 1.62	8.39	1.73

[a]The DM total mass is calculated using the last RC data point in the halo for r.
[b]The DM total mass is calculated using the scale radius r_0.

In addition, namely the χ^2 and the BIC, are reported for each halo profile. The quantities obtained from the fits show that ESO0140040 has a more massive halo than the other two galaxies. Its virial mass exceeds

those of ESO3050090 and ESO4880049. This difference explains why ESO0140040 achieves higher velocities and why its RC extends to larger radii.

The statistical analysis of the RCs carried out using both the MCMC approach and the nonlinear fitting procedure leads to conclusion: the King halo profile provides a better fit to the observed RCs than the Plummer model. In the case of ESO0140040, the MCMC results reported in Table 1 show that, for $N = 8$ data points and $k = 2$ free parameters, the BIC yields $BIC = 9.12$ for the King profile and $\mathrm{BIC} = 13.34$ for the Plummer profile. Adopting $\mathrm{BIC}_{min} = 9.12$ as the reference value, the corresponding relative criterion is $\Delta\mathrm{BIC} = 4.22$ for the Plummer model. The nonlinear fitting results reported in Table 2 are consistent with this outcome, as the King profile yields both a lower χ^2 and a smaller BIC than the Plummer model.

A similar behavior is observed for ESO3050090. As shown by the MCMC analysis in Table 3, the BIC yields $\mathrm{BIC} = 6.37$ for the King profile and $\mathrm{BIC} = 6.50$ for the Plummer profile for $N = 16$, corresponding to $\Delta\mathrm{BIC} = 0.13$ for the latter. Although the difference is small, the King halo profile is slightly favored. This behavior is also observed in the nonlinear fitting results reported in Table 4, where the King model yields the lowest BIC value. An analogous result is obtained for ESO4880049. The MCMC analysis summarized in Table 5 yields $\mathrm{BIC} = 5.61$ for the King profile and $\mathrm{BIC} = 6.53$ for the Plummer profile for $N = 11$, leading to ΔBIC=0.92 for the Plummer model. The nonlinear fitting analysis presented in Table 6 leads to the same qualitative conclusion, as the King profile exhibits a substantially lower BIC value than the Plummer model.

Overall, the results presented in the tables enable a clear comparison of the ability of the different halo profiles to reproduce the observed RCs, while the derived virial masses and radii provide a physically meaningful description of the DM halos.

5. Conclusion

In this work we analyzed the RCs of the LSB spiral galaxies ESO3050090, ESO4880049, and ESO0140040 within the two cored DM halo models: the King and Plummer profiles. By combining MCMC method with nonlinear least-squares fitting, we constrained the structural parameters (ρ_0 and r_0), derived the corresponding mass distributions, and performed a comparison of two models using the BIC.

The main result is that both profiles reproduce the observed RCs within the measurement errors over the entire radial range covered by the data. This demonstrates that, these galaxies are dominated by a dark halo component whose gravitational potential alone can account for the observed circular velocities under the assumption $v_{tot}^2 \simeq v_{profile}^2$.

Despite the general similarity of the fitting results, statistical comparison showed that the King profile is preferred over the Plummer profile, with the strength of the preference depending on the galaxy. For ESO0140040, the difference in BIC indicates positive evidence in favor of King, while for ESO3050090 and ESO4880049 the evidence is weaker. In particular, for ESO3050090 and ESO4880049, the MCMC-based ΔBIC values of 0.13 and 0.92 are below the conventional threshold of 2 and should be interpreted as negligible to weak preference. However, the nonlinear fitting yields ΔBIC = 2.28 and 8.39 for these galaxies, lending additional support to the King model. Taken together, both methods consistently favor the King profile, though the strength of this preference varies across the sample.

These results have a following physical interpretation: the shallower outer density decline of the King model ($\rho_K \sim r^{-3}$) implies a more extended mass distribution that better supports the observed velocities at larger radii. It worth noting that galaxies ESO3050090, ESO4880049 and ESO0140040 were previously investigated within the sample of LSB galaxies in the framework of SFDM model [26], brane-world gravity [27] and nearly Newtonian approximation [28]. Although these models imply different physical interpretation (via specific parameters), they produce rotation curves comparable to those obtained in present work. In addition, the derived central densities and characteristic halo radii are consistent with the values inferred here. This agreement indicates that the observational data for given galaxies primarily constrain the overall gravitational potential. However, the divergence between different approaches may become more pronounced in the halos of larger galaxies.

In general, the results of a present work show that cored DM halos provide a self-consistent and adequate description of the kinematics of considered LSB galaxies. The preference for cored profiles found in this work is consistent with the general trend reported in the literature for LSB galaxies, but should not be interpreted as evidence against CDM cuspy profiles. To draw statistically robust conclusions about the preference between cored and cuspy profiles, a direct fitting comparison must be performed on a significantly larger and

morphologically diverse galaxy sample, with high-resolution Rotation Curve data extending to large radii where the two profile families predict the most distinct kinematic signatures.

For a more detailed analysis of different core DM profiles, it would be interesting to construct RCs for galaxies extending to larger radii and to include the impact of their baryonic component and inner structure. These aspects are of our further interest.

Conflict of interest statement

The authors declare that they have no conflict of interest in relation to this research, whether financial, personal, authorship or otherwise, that could affect the research and its results presented in this paper.

CRediT author statement

Kurmanov Ye.: Conceptualization, Methodology, Supervision; **Konysbayev T.**: Software, Validation; **Suliyeva G.**: Formal analysis, Writing - Review & Editing; **Urazalina A.**: Formal analysis, Writing - Review & Editing; **Oteev T.**: Formal analysis, Writing - Review & Editing; **Rabigulova G.**: Investigation, Writing - Original Draft; **Nurlanbek U.**: Investigation, Writing - Original Draft; **Adil M.**: Investigation, Writing - Original Draft; **Bekmurat B.**: Investigation, Writing - Original Draft; **Tuzen G.**: Investigation, Writing - Original Draft. The final manuscript was read and approved by all authors.

Statement on the use of Artificial Intelligence.

During the preparation of this manuscript, artificial intelligence tools were used solely for language editing and grammatical improvement. No AI tools were used to generate scientific content, analysis, results, or conclusions.

Data Availability Statement

The data are available upon reasonable request from the authors.

Funding

This research was funded by the Science Committee of the Ministry of Science and Higher Education of the Republic of Kazakhstan (Grant No. AP23488743).

References

1 Planck Collaboration (2020). Planck 2018 results. *Astron. Astrophys.* 641, A6, https://doi.org/10.1051/0004-6361/201833910, 1807.06209.

2 Lake, G. (1989). Must the Disk and Halo Dark Matter Be Different? *Astronomical Journal*. 98, 1554, https://doi.org/10.1086/115238.

3 Lux, H., Read, J. I., Lake, G., Johnston, K. V. (2012). The Multidimensional Milky Way. *Mon. Not. Roy. Astr. Soc.*, 424(1), L16–L20. https://doi.org/10.1111/j.1745- 3933.2012

4 Deason, A. J., Belokurov, V., Sanders, J. L. (2019). The total stellar halo mass of the Milky Way. *Mon. Not. Roy. Astr. Soc.*, 490(3), 3426–3439. https://doi.org/10.1093/mnras/stz2793, 1908.02763.

5 de Blok, W. J. G. (2010). The Core-Cusp Problem. *Advances in Astronomy*, 789293, https://doi.org/10.1155/2010/789293, 0910.3538.

6 Seo, G., Sohn, J., Lee, M. G. (2020). Tracing Dark Matter Halos with Satellite Kinematics and the Central Stellar Velocity Dispersion of Galaxies. *Astrophys. J.*, 903(2), 130. https://doi.org/10.3847/1538-4357/abbd92, 2010.00693.

7 Rubin, V. C., Ford, Jr. W. K., Thonnard, N. (1980). Rotational properties of 21 SC galaxies with a large range of luminosities and radii, from NGC 4605 (R=4kpc) to UGC 2885 (R=122kpc). *Astrophys. J.*, 238, 471–487. https://doi.org/10.1086/158003

8 Volders, L. M. J. S. (1959). Neutral hydrogen in M 33 and M 101. *Bulletin of the Astronomical Institutes of the Netherlands*, 14, 323. https://scholarlypublications.universiteitleiden.nl/handle/1887/6267.

9 Freeman, K. C. (1970). On the Disks of Spiral and S0 Galaxies. *Astrophys. J.* 160, 811. https://doi.org/10.1086/150474

10 Navarro, J. F., Frenk, C. S., White, S. D. M. (1996). The Structure of Cold Dark Matter Halos. *Astrophys. J.* 462, 563-575. https://doi.org/10.1086/177173

11 Burkert, A. (1995). The Structure of Dark Matter Halos in Dwarf Galaxies. *Astrophys. J. Lett.* 447, L25–L28. https://doi.org/10.1086/309560, astro-ph/9504041.

12 Jimenez, R., Verde, L., Oh, S. P. (2003). Dark halo properties from rotation curves. *Mon. Not. Roy. Astr. Soc.*, 339(1), 243–259. https://doi.org/10.1046/j.1365-8711.2003.06165.x

13 Brownstein, J. R., Moffat, J. W. (2006). Galaxy Rotation Curves without Nonbaryonic Dark Matter. *The Astrophysical Journal*, 636(2), 721. https://doi.org/10.1086/498208.

14 Boshkayev, K., Konysbayev, T., Kurmanov, Y., Muccino, M., G. Z. (2020). Physical properties of dark matter in galaxy U11454. *Physical Sciences and Technology*, 10(3-4), 11–20. https://doi.org/10.26577/PHST.2020.V7.I2.02

15 Kurmanov, Y., Boshkayev, K., Konysbayev, T., Muccino, M., Urazalina, A., Ikhsan, G., Saiyp, N., Rabigulova, G., Karlinova, M., Suliyeva, G., Beissen, N. (2023). Analysis of dark matter profiles in the halos of spiral galaxies. *Physical Sciences and Technology*, 10(3-4), 4–16. https://doi.org/10.26577/PHST.2023.V10.I2.01

16 Boshkayev, K., Konysbayev, T., Kurmanov, E., Luongo, O., Muccino, M. (2020). Imprint of Pressure on Characteristic Dark Matter Profiles: The Case of ESO0140040. *Galaxies*, 8(4), 74. https://doi.org/10.3390/galaxies8040074.

17 Boshkayev, K., Konysbayev, T., Kurmanov, Y., Luongo, O., Muccino, M., Quevedo, H., Zhumakhanova, G. (2024). Numerical analyses of M31 dark matter profiles. *International Journal of Modern Physics D*, 33, 2450016. https://doi.org/10.1142/S0218271824500160, 2212.02999.

18 Boshkayev, K., Konysbayev, T., Kurmanov, E., Luongo, O., Malafarina, D., Mutalipova, K., Zhumakhanova, G. (2021). Effects of non-vanishing dark matter pressure in the Milky Way Galaxy. *Mon. Not. Roy. Astr. Soc.*, 508(1), 1543–1554. https://doi.org/10.1093/mnras/stab2571, 2107.00138.

19 Suliyeva, G., Kurmanov, Y., Konysbayev, T., Boshkayev, K., Urazalina, A., Luongo, O. (2024). Finite temperature effects within scalar field dark matter model. *Eurasian Physical Technical Journal*, 21(2(48)), 92–101. https://doi.org/10.31489/2024No2/92-101.

20 de Blok, W. J. G., McGaugh, S. S., Rubin, V. C. (2001). High-Resolution Rotation Curves of Low Surface Brightness Galaxies. II. Mass Models. *Astronomical Journal*, 122(5), 2396–2427. https://doi.org/10.1086/323450.

21 Mannheim, P. D., O'Brien, J. G. (2012). Fitting galactic rotation curves with conformal gravity and a global quadratic potential. *Phys. Rev. D*, 85(12), 124020. https://doi.org/10.1103/PhysRevD.85.124020, 1011.3495.

22 de Blok, W. J. G., Bosma, A. (2002). High-resolution rotation curves of low surface brightness galaxies. *Astron. Astrophys.*, 385, 816–846. https://doi.org/10.1051/0004-6361:20020080.

23 Barranco, J., Bernal, A., Nunez, D. (2015). Dark matter equation of state from rotational curves of galaxies. *Mon. Not. Roy. Astr. Soc.*, 449(1), 403–413. https://doi.org/10.1093/mnras/stv302

24 King, I. (1962). The structure of star clusters. I. an empirical density law. *Astronomical Journal*, 67, 471. https://doi.org/10.1086/108756

25 Plummer, H. C. (1911). On the problem of distribution in globular star clusters. *Mon. Not. Roy. Astr. Soc.*, 71, 460–470. https://doi.org/10.1093/mnras/71.5.460.

26 Fernandez-Hernandez, L. M., Rodrıguez-Meza, M. A., Matos, T. (2018). Comparison between two scalar field models using rotation curves of spiral galaxies. *Journal of Physics Conference Series*, 1010, 012005. https://doi.org/10.1088/1742-6596/1010/1/012005

27 Garcia-Aspeitia, M. A., Rodriguez-Meza**M** M. A. (2018). Constraining brane tension using rotation curves of galaxies. *Journal of Physics Conference Series*, 1010, 012006. https://doi.org/10.1088/1742-6596/1010/1/012006.

28 Capistrano, A. J. S., Barrocas, G. R. G. (2018). Rotation curves of LSBGs and dwarf galaxies in a nearly Newtonian solution. *Mon. Not. Roy. Astr. Soc.*, 475(2), 2204–2214. https://doi.org/10.1093/mnras/stx2909.

AUTHORS' INFORMATION

Kurmanov Yergali - PhD, Associate Professor, Al-Farabi Kazakh National University, Almaty, Kazakhstan; SCOPUS Author ID: 57695578100, https://orcid.org/0000-0003-3695-0166; ergaly_90@mail.ru

Konysbayev Talgar - PhD, Senior Researcher Associate, Al-Farabi Kazakh National University, Almaty, Kazakhstan; SCOPUS Author ID: 57219800003, https://orcid.org/0000-0001-9476-3700; talgar_777@mail.ru

Suliyeva Gulnara - PhD, Junior Research Associate, Al-Farabi Kazakh National University, Almaty, Kazakhstan; SCOPUS Author ID: 57818572500, https://orcid.org/0000-0001-5072-7898; g_suliyeva@mail.ru

Urazlaina Ainur - PhD, Senior Lecturer, Al-Farabi Kazakh National University, Almaty, Kazakhstan; SCOPUS Author ID: 57076979300, https://orcid.org/0000-0002-4633-9558; y.a.a.707@mail.ru

Oteev Tursinbay - PhD, Teaching Assistant, Nukus State Pedagogical Institute, Nukus, Uzbekistan; SCOPUS Author ID: 57190254652, https://orcid.org/0000-0002-5733-834X; oteevtp@gmail.com

Rabigulova Guldana – PhD student, Al-Farabi Kazakh National University, Almaty, Kazakhstan; SCOPUS Author ID: 58848753900, https://orcid.org/0009-0003-8998-6282; guldanaberikhanovna@gmail.com

Nurlanbek Ulpan - PhD student, Al-Farabi Kazakh National University, Almaty, Kazakhstan; https://orcid.org/0009-0005-7107-5899; ulpan.nurlanbek02@gmail.com

Adil Makhabbat - Master student, Al-Farabi Kazakh National University, Almaty, Kazakhstan; https://orcid.org/0009-0008-2202-4413; adilmahabbat@gmail.com

Bekmurat Bagzhan - Master student, Al-Farabi Kazakh National University, Almaty, Kazakhstan; https://orcid.org/0009-0008-0000-442X; Bagzhan159@gmail.com

Tuzen Galiya - Master student, Al-Farabi Kazakh National University, Almaty, Kazakhstan; https://orcid.org/0009-0001-5083-9395; galiyatuzen@gmail.com